Multiwavelength surface contouring from phase-coded diffraction patterns

Multiwavelength surface contouring from phase-coded diffraction patterns

Vladimir Katkovnik[1], Igor Shevkunov[1,2,*], Nikolay V. Petrov[2], and Karen Egiazarian[1]

[1]Department of Signal Processing, Technology University of Tampere, Finland
[2]Department of Photonics and Optical Information Technology, ITMO University, St. Petersburg, Russia

ABSTRACT

We propose a new algorithm for absolute phase retrieval from multiwavelength noisy phase coded diffraction patterns in the task of surface contouring. A lensless optical setup is considered with a set of successive single wavelength experiments. The phase masks are applied for modulation of the multiwavelength object wavefronts. The algorithm uses the forward and backward propagation for coherent light beams and sparsely encoding wavefronts which leads to the complex-domain block-matching 3D filtering. The key-element of the algorithm is an original aggregation of the multiwavelength object wavefronts for high-dynamic-range profile measurement. Numerical experiments demonstrate that the developed approach leads to the effective solutions explicitly using the sparsity for noise suppression and high-accuracy object profile reconstruction.

Keywords: Multiwavelength phase retrieval, absolute phase retrieval, surface contouring, phase imaging, discrete optical signal processing

1. INTRODUCTION

Holography and interferometry are techniques to record object amplitude and phase information using interference of object and reference light beams. These records called holograms or interferograms provide data sufficient for reconstruction of object 3D image using the diffraction theory (e.g. Refs. 1–3).

Diffraction imaging being similar to holography differs first of all by lack of reference beams. In many lensless setups information on the object is given by the phase coded diffraction patterns registered at the image plane. In these intensity measurements the phase information of registered wave-fields is eliminated. The problem of the object reconstruction is well known as the phase retrieval where "phase" emphasizes that the missing phase defines the main difficulties of the problem and its principal difference with respect to holography.

It is well known that the phase retrieval is from the class of the challenging ill-posed problems especially difficult for noisy observations. The phase/observation diversity sufficient for reliable reconstruction of the object phase from the intensity patterns is a crucial moment of the phase retrieval problems. Defocusing and phase modulation are known as effective instruments in order to achieve the desirable diversity (e.g. Refs. 4–7). Various types of the diffraction optical elements can be used for design of the diffraction phase imaging systems.[8]

The Gerchberg-Saxton (GS) phase retrieval algorithms[9,10] are from the most popular in the field. These iterative algorithms originally proposed for the noiseless data use alternating projection between the complex-valued object u_o and variables u_s at the sensor plane. In these iterations the amplitudes in u_s are replaced by square roots of the corresponding items of the measurements. The back projection of the u_s to the object u_o is modified according to the prior information on the object, e.g. support size and shape, amplitude value, etc. The GS algorithms exist in many modifications.[11,12] The review and analysis of this type of the algorithms as well as further developments can be found in Ref. 13.

Many publications concern revisions of the GS algorithms by using optimization formulations. In particular, the links between the conventional GS and variational techniques are studied in Refs. 14–16. Contrary to the

Further author information: (Send correspondence to I.Shevkunov)
I.Shevkunov: e-mail: Igor.Shevkunov@tut.fi, N.V.Petrov: e-mail: n.petrov@niuitmo.ru,
V.Katkovnik: e-mail:vladimir.katkovnik@tut.fi, K.Egiazarian: e-mail: karen.egiazarian@tut.fi.

intuitively clear heuristic of the GS algorithms, the variational approaches usually have a stronger mathematical background including image formation modeling, formulation of the objective function (criterion) and finally going to numerical techniques solving corresponding optimization tasks.

We wish refer also to the recent overview[17] concentrated on the algorithms for the phase retrieval with the Fourier transform measurements and applications in optics. The constrains sufficient for uniqueness of the solution are presented in detail. Beyond the alternating projection of GS the novel mathematical methods are discussed: semidefinite programming phase lifting using matrix completion *(PhaseLift algorithm)*[18] and greedy sparse phase retrieval (*GESPAR algorithm*).[19] The fundamental progress for the methods based on the convex matrix optimization is announced in Ref. 20, where the novel algorithm is presented named "Sketchy Decisions". This algorithm allows to deal with high dimensions typical for the phase-lifting methods and is supported by the mathematical analysis with the convergence proof.

In this brief overview, especially we wish to note the recent Wirtinger flow (WF) algorithms presented in Refs. 21,22. These algorithms are iterative complex domain gradient descents applied to Gaussian and Poissonian likelihood criteria.

The techniques based on the proximity operators developed in Refs. 23 and 24 provide a regularized optimization of the maximum likelihood criteria also for both Gaussian and Poissonian observations. The sparsity based techniques is a hot topic in phase retrieval (e.g. Ref. 19). The transform domain phase/amplitude sparsity for the phase imaging is developed in Refs. 25–27. For the phase retrieval these techniques are applied in Refs. 28–30. A sparse dictionary learning for phase retrieval is developed in Ref. 31.

In recent years, there has been an increase in demand for multispectral imaging. Multispectral information by recording object waves with multiple wavelengths that are irradiated from multiwavelength/color light sources helps to analyze and recognize objects, to clarify color and tissue distributions of an object and dramatically improve the quality of imaging. Multiwavelength digital holography has an enhanced ability for 3D wide-range shape measurements by using multiwavelength phase unwrapping, due to the recording of quantitative phase information with multiple wavelengths. In phase retrieval the multiwavelength is an effective instrument enabling good phase/data diversity.

The multiwavelength phase retrieval is much less studied as compared with the standard single-wavelength formulation. These works by the principle of measurements can be separated in two groups. In the first one, the absolute phase is estimated from phase measurements obtained in some or another way. This scenario is typical for interferometry/holography where reference beams are applied to reveal the phase information, e.g. Refs. 32–36. The phase unwrapping algorithms for $2D$ images with simultaneous processing of multiple noisy complex-exponent observations have been developed based on the maximum likelihood techniques.[37,38]

Another group of the techniques use as measurements amplitudes or intensities (powers). These formulations are from the class of the multiwavelength phase retrieval problems, e.g. Refs. 39–44. The Chinese Remainder Theorems provide a class of the methods with a good theoretical background.[45] The reformulation of these approaches for more practical scenarios with noisy data and for robust estimation lead to the techniques similar to various forms of the maximum likelihood.[46,47]

In this paper we develop an approach which can be treated as a development of the SPAR algorithms[28,29] and the maximum likelihood absolute phase reconstruction for multiwavelength observations.[38] The use of multiple wavelengths allows to overcome the impossibility of the phase unwrapping in the cases when objects' relief contains a fast oscillating peaks exceeding wavelength range and/or the observations are strongly affected by noise.

2. OPTICAL SETUP AND IMAGE FORMATION MODEL

2.1 Multiwavelength object and image modeling

We will present our algorithm in a framework of solving the problem of relief measurement of a transparent object. Since the task of surface contouring is similar both aspects of transparent and reflecting objects are,[39] so the model developed below can be applied to both types of objects. In the framework of this paper we consider in

details a more interesting case of the transparent object with dispersion of the refractive index, because ignoring of this dependence can cause significant distortions in the profile of the object being reconstructed.[48]

Let $h_o(x)$, $x \in R^2$, be a profile of transmission $2D$ object to be reconstructed. A coherent multiwavelength light beam generates corresponding complex-valued wavefronts $u_{o,\lambda} = b_{o,\lambda}\exp(j\varphi_{o,\lambda})$, $\lambda \in \Lambda$, where Λ is a set of the wavelengths and $\varphi_{o,\lambda} = \dfrac{2\pi}{\lambda}h_o(n_\lambda - 1)$ are phase delays corresponding to h_o, where n_λ is the refractive index.

In the lensless phase retrieval the problem at hand is a reconstruction of the profile $h_o(x)$ from the noisy observations of diffractive patterns, registered at some distance from the object. For the high magnitude variation of h_o the corresponding absolute phases $\varphi_{o,\lambda}$ take values beyond the basic phase interval $[0, 2\pi]$, then only wrapped phases can be obtained from $u_{o,\lambda}$.

We demonstrate that the multiwavelength setup allows to reconstruct the profile of the objects, which height variations are significantly greater than used wavelengths, as well as the corresponding absolute phases. In what follows, we apply the following convenient notation for object modeling:

$$u_{o,\lambda} = b_{o,\lambda}\exp(j\mu_\lambda\varphi_o),\ \lambda \in \Lambda, \tag{1}$$

where $u_{o,\lambda}(x) \in \mathbb{C}^2$, $\varphi_o(x) \in R^2$ is the object absolute phase in radians, $\mu_\lambda > 0$ are dimensionless relative frequencies and $\Lambda = [\lambda_o, \lambda_1, ..., \lambda_{n_\lambda - 1}]$ is the set of the wavelengths.

The link with the previous notation is obvious: $\mu_\lambda = \dfrac{\lambda'(n_\lambda - 1)}{\lambda(n_{\lambda'} - 1)}$ and

$$\varphi_o = \frac{2\pi}{\lambda'}h_o(n_{\lambda'} - 1). \tag{2}$$

Here $\lambda' \in \Lambda$ is a reference wavelength and φ_o is an absolute phase corresponding to this wavelength.

We are interested in two-dimensional imaging and assume that amplitude, phase and other variables in what follows are functions of the argument x given on the regular $2D$ grid.

The parameter μ_λ establishes a link between the absolute phase φ_o and the wrapped phase $\psi_{o,\lambda}$ of $u_{o,\lambda}$ which can be measured at the λ-channel. The wrapped phase is related with the true absolute phase, φ_o, as $\mu_\lambda\varphi_o = \psi_{o,\lambda} + 2\pi k_\lambda$, where k_λ is an integer, $\psi_{o,\lambda} \in [-\pi, \pi)$. The link between the absolute and wrapped phase conventionally is installed by the wrapping operator $\mathcal{W}(\cdot)$ as follows:

$$\psi_{o,\lambda} = \mathcal{W}(\mu_\lambda\varphi_o) \equiv \mathrm{mod}(\mu_\lambda\varphi_o + \pi, 2\pi) - \pi. \tag{3}$$

$\mathcal{W}(\cdot)$ decomposes the absolute phase $\mu_\lambda\varphi_o$ into two parts: the fractional part $\psi_{o,\lambda}$ and the integer part defined as $2\pi k_\lambda$.

The image and observation modeling is defined as

$$\begin{aligned} u_{s,\lambda} &= \mathcal{P}_{s,\lambda,d}\{u_{o,\lambda}\}, & (4)\\ y_{s,\lambda} &= |u_{s,\lambda}|^2, & (5)\\ z_{s,\lambda} &= \mathcal{G}\{y_{s,\lambda}\},\ s = 1, ..., S,\ \lambda \in \Lambda, & (6) \end{aligned}$$

where $u_{s,\lambda}$ is a wavefront propagated to the sensor plane, $\mathcal{P}_{s,\lambda,d}\{\}$ is an image (diffraction pattern) formation operator, i.e. the propagation operator from the object to the sensor plane, including in particular random phase masks used for wavefront modulation; d is a propagation distance; $y_{s,\lambda}$ is the intensity of the wavefront at the sensor plane and $z_{s,\lambda}$ are noisy observations as defined by the generator $\mathcal{G}\{\}$ of the random variables corresponding to $y_{s,\lambda}$, S is a number of experiments.

The considered multiwavelength phase retrieval problem consists in reconstruction of φ_o and $b_{o,\lambda}$ from the observation $z_{s,\lambda}$ provided that μ_λ, $\mathcal{P}_{s,\lambda,d}\{\}$ and $\mathcal{G}\{\}$ are known. If the phases $\mu_\lambda\varphi_o \in [\pi, -\pi)$, the problem

becomes nearly trivial as estimates of $\mu_\lambda \varphi_o$ and $b_{o,\lambda}$ can be found processing data separately for each λ by any phase retrieval algorithm applicable for complex-valued object, in particular by the SPAR algorithm.[49] It gives for us the estimates of $b_{o,\lambda}$ and $\mu_\lambda \varphi_o$ directly. These estimates of $\mu_\lambda \varphi_o(x)$ are biased as the intensities $y_{s,\lambda}$ are insensitive with respect to invariant shifts in φ_o. We will represent these estimates in the form $\mu_\lambda \varphi_o(x) + \delta_\lambda$, where δ_λ are invariant on x.

The problem becomes nontrivial, much more interesting and challenging when the object phases $\mu_\lambda \varphi_o$ go beyond the range $[\pi, -\pi)$ and the phase unwrapping is imbedded in the multiwavelength phase retrieval.

This paper is focused on the reconstruction of the absolute phase φ_o. Multiple single wavelength experiments are produced with the results registered by a wide-band gray-scale CCD sensor. The measurements are of the form:

$$y_{s,\lambda}(x) = |u_{s,\lambda}(x)|^2,\ z_{s,\lambda}(x) = \mathcal{G}\{y_{s,\lambda}(x)\}, \tag{7}$$

$$x \in \Omega,\ \lambda \in \Lambda,\ s = 1, ..., S, \tag{8}$$

where Ω is a set of the sensor pixels.

A single wavelength is used for each experiment and the obtained observations $\{z_{s,\lambda}\}$ are used jointly for reconstruction of $\varphi_o(x)$ and $h_o(x)$.

2.2 Noisy observation

The measurement process in optics amounts to count the photons hitting the sensor's elements and is well modeled by independent Poisson random variables (e.g. Refs. 24, 50, 51). In many applications in biology and medicine the radiation (laser, X-ray, etc.) can be damaging for a specimen. Then, the dose (energy) of radiation can be restricted by a lower exposure time or by use a lower power radiation source, say up to a few or less numbers of photons per pixel of sensor what leads to heavily noisy registered measurements. Imaging from these observations, in particular, phase imaging is called photon-limited.

The probability that a random Poissonian variable $z_{s,\lambda}(x)$ of the mean value $y_{s,\lambda}(x)$ takes a given non-negative integer value k, is given by

$$p(z_{s,\lambda}(x) = k) = \exp(-y_{s,\lambda}(x)\chi)\frac{(y_{s,\lambda}(x)\chi)^k}{k!}, \tag{9}$$

where $y_{s,\lambda}(x)$ is the intensity of the wavefront at the pixel x.

Recall that the mean and the variance of Poisson random variable $z_{s,\lambda}(x)$ are equal and are given by $y_{s,\lambda}(x)\chi$, i.e., $E\{z_{s,\lambda}(x)\} = \mathrm{var}\{z_{s,\lambda}(x)\} = y_{s,\lambda}(x)\chi$, here $E\{\}$ is a mathematical expectation, $\mathrm{var}\{\}$ is a variance. Defining the observation signal-to-noise ratio (SNR) as the ratio between the square of the mean and the variance of $z_{s,\lambda}(x)$, we have $SNR = E^2\{z_{s,\lambda}(x)\}/\mathrm{var}\{z_{s,\lambda}(x)\} = y_{s,\lambda}(x)\chi$. Thus, the relative noisiness of observations becomes stronger as $\chi \to 0$ ($SNR \to 0$) and approaches zero when $\chi \to \infty$ ($SNR \to \infty$). The latter case corresponds to the noiseless scenario: $z_{s,\lambda}(x)/\chi \to y_{s,\lambda}(x)$ with the probability equal to 1.

The parameter $\chi > 0$ in (9) is a scaling factor defining a proportion between the intensity of the observations with respect to the intensity of the input wavefront. This parameter is of importance as it controls a level of the noise in observations. Physically it can be interpreted as an exposure time and as the sensitivity of the sensor with respect to the input radiation.

In order to make the noise more understandable the noise level can be characterized by the estimates of SNR

$$SNR_\lambda = 10 \log_{10} \frac{\chi^2 \sum_{s=1}^{S} ||y_{s,\lambda}||_2^2}{\sum_{s=1}^{S} ||y_{s,\lambda}\chi - z_{s,\lambda}||_2^2},\ dB \tag{10}$$

and of the mean value of photons per pixel:

$$N_{photon,\lambda} = \sum_x z_{s,\lambda}(x)/N_{sensor}. \tag{11}$$

Here N_{sensor} is a number of sensor pixels. Smaller values of χ lead to smaller SNR and N_{photon}, i.e. to noisier observations $z_{s,\lambda}(x)$.

3. DEVELOPMENT OF ALGORITHM

We consider the problem of the absolute phase retrieval as an estimation of $u_o \in \mathbb{C}^n$ from noisy observations $\{\mathbf{z}_{s,\lambda}\}$. This problem is rather challenging mainly due to the periodic nature of the likelihood function with respect to the phase φ_o and the non-linearity of the observation model. Provided a stochastic noise model with independent samples, the maximum likelihood leads to the basic criterion function

$$\mathcal{L}_0 = \sum_{\lambda\in\Lambda}\sum_{s=1}^{S}\sum_{x\in\Omega} l(z_{s,\lambda}(x), |u_{s,\lambda}(x)|^2), \tag{12}$$

where $l(z, |u|^2)$ denotes the minus log-likelihood of a candidate solution for u_o given through the observed true intensity $|u|^2$ and noisy outcome z.

For the Poissonian distribution we have $l(z, |u|^2) = |u|^2\chi - z\log(|u|^2\chi)$. In (12) s and x denote the experiment number and pixels of variables, respectively.

Including the image formation model (4) and amplitude/phase modeling of the object (1) by the penalty quadratic norms of the residuals we introduce the following extended criterion:

$$\begin{aligned}&\mathcal{L}(u_{s,\lambda},\, u_{o,\lambda},\, b_o,\, \varphi_o\,,\, \delta_\lambda) = \\ &\sum_{\lambda,s,x} l(z_{s,\lambda}(x), |u_{s,\lambda}(x)|^2) + \frac{1}{\gamma_1}\sum_{\lambda,s}||u_{s,\lambda} - \mathcal{P}_{s,\lambda}u_{o,\lambda}||_2^2 + \frac{1}{\gamma_2}\sum_{\lambda}||b_{o.\lambda}\exp(j(\mu_\lambda\cdot\varphi_o + \delta_\lambda)) - u_{o,\lambda}||_2^2,\end{aligned} \tag{13}$$

where $\gamma_1, \gamma_2 > 0$ are regularization parameters, and $||\cdot||_2^2$ stands for the Hadamard norm.

Remind, that phase retrieval algorithms may reconstruct the phase φ_o only within an invariant additive error. The corresponding phase errors for different wavelength are modeled in (13) by δ_λ as unknown phase-shift parameters.

We say that the object complex exponents of different wavelengths are in-phase (or synchronized) if $\delta_\lambda = 0$, $\lambda \in \Lambda$, and out-of-phase if some of $\delta_\lambda \neq 0$. For proper estimation of φ_o, these phase-shifts δ_λ should be estimated and compensated.

The criterion $\mathcal{L}$ is minimized with respect to $u_{s,\lambda}$, $u_{o,\lambda}$, b_o, φ_o as well as with respect to the phase-shifts δ_λ in order to get the proper estimates of the main variables.

1. Minimization with respect to $u_{s,\lambda}$ concerns the first two summands in $\mathcal{L}$. The problem is additive on λ and x and, respectively, can be obtained separately for each λ and x. The corresponding analytical solution is obtained in Ref. 28. This solution defines $u_{s,\lambda}$ as functions of noisy observation $z_{s,\lambda}$ and the projection $\mathcal{P}_s u_{o,\lambda}$ of $u_{o,\lambda}$ on the sensor. The amplitudes of $u_{s,\lambda}$ are updated accordingly to given observations and the phases are preserved.

2. Minimization with respect to $u_{o,\lambda}$ goes to the last two summands of the criterion. It is a quadratic problem with the solution of the form

$$\hat{u}_{o,\lambda} = (\sum_s \mathcal{P}^*_{s,\lambda}\mathcal{P}_{s,\lambda} + I\gamma_1/\gamma_2)^{-1} \times (\sum_s \mathcal{P}^*_{s,\lambda}u_{s,\lambda} + \gamma_1/\gamma_2 b_{o,\lambda}\exp(j\mu_\lambda\varphi_o)), \tag{14}$$

where I stands for the identity operator.

Here the operator $\mathcal{P}^*_{s,\lambda}$ is Hermitian adjoint for $\mathcal{P}_{s,\lambda}$. If $\mathcal{P}_{s,\lambda}$ are orthonormal such that $\sum_s \mathcal{P}^*_{s,\lambda}\mathcal{P}_{s,\lambda}$ is the identity operator, $\sum_s \mathcal{P}^*_{s,\lambda}\mathcal{P}_{s,\lambda} = I$, then the solution is simplified to the form

$$\hat{u}_{o,\lambda} = \frac{\sum_s \mathcal{P}^*_s u_{s,\lambda} + \gamma_1/\gamma_2 b_{o,\lambda}\exp(j\mu_\lambda\varphi_o)}{1 + \gamma_1/\gamma_2}. \tag{15}$$

3. Minimization on $b_{o,\lambda}$, φ_o and δ_λ (the last summand in the criterion) is the non-linear least square fitting of the wavelength dependent $u_{o,\lambda}$ by the object phase φ_o invariant with respect λ, amplitudes $b_{o,\lambda}$ and spatially invariant phase-shifts δ_λ. The criterion for this problem can be given in the equivalent form as

$$\mathcal{L}_1(b_{o,\lambda},\, \varphi\,,\ \delta_\lambda) = \sum_\lambda ||b_{o.\lambda} \exp(j(\mu_\lambda \cdot \varphi_o)) - |u_{o,\lambda}| \exp(j(\psi_{o,\lambda} - \delta_\lambda))||_2^2, \tag{16}$$

where $\psi_{o,\lambda} = angle(u_{o,\lambda})$, i.e. the wrapped phase of $u_{o,\lambda}$.

In this representation the phase shifts δ_λ are addressed to the wrapped phases $\psi_{o,\lambda}$ in order to stress that the complex exponents $\exp(j(\psi_{o,\lambda}))$ can be out-of-phase with $\exp(j(\mu_\lambda \cdot \varphi_o))$ and the variables δ_λ serve in order to compensation this phase difference and make the phase modeling of the object by $\exp(j(\mu_\lambda \cdot \varphi_o))$ corresponding to the complex exponent $\exp(j(\psi_{o,\lambda}))$.

The assumption $b_{o.\lambda} \simeq |u_{o,\lambda}|$ is supported in our algorithm implementation by the initialization procedure enabling the high accuracy estimation of the amplitudes $|u_{o,\lambda}|$ in processing of separate wavelength observations.

The Absolute Phase Reconstruction (APR) algorithm is developed for minimization of $\mathcal{L}_1$ on φ_o and δ_λ. The derivation and details of this algorithm are presented in Appendix.

3.1 Algorithm's implementation

Using the above solutions the iterative algorithm is developed of the structure shown in Table I. The initialization by the complex-valued $u^1_{o,\lambda}$ is obtained from the observations $\{z_{s,\lambda}\}$ by the SPAR algorithm[28] separately for each wavelength. The main iterations start from the forward propagation (Step 1) and follows by the amplitude update for $u^t_{s,\lambda}$ at Step 2. The operator Φ_1 derived in Ref. 28 is presented below. The back propagation is realized in Step 3, and the operator Φ_2 is defined by (15). The absolute phase reconstruction from the wrapped phases of $u^{t+1}_{o,\lambda}$ is produced in Step 4 by the *APR* algorithm presented in Appendix. It is based on the grid optimization with respect to φ_o and the phase-shifts $\delta_{\lambda'}$ for the reference channel λ'.

The obtained amplitude and phase update $u^{t+1}_{o,\lambda}$ at Step 5. The number of iteration is fixed in this implementation of the algorithm. The Steps 3 and 4 are completed by the Block-Matching 3-D (BM3D) filtering.[49] In Step 3 it is the filtering of complex-valued $u^{t+1/2}_{o,\lambda}$ produced separately for the wrapped phase and amplitude of $u^{t+1/2}_{o,\lambda}$. In Step 4 this filtering is applied to the absolute phase $\varphi^{t+1/2}_o$. These BM3D filters are derived from the group-wise sparsity priors for the filtered variables. This technique is based on the Nash equilibrium formulation for the phase retrieval instead of the more conventional constrained optimization with a single criterion function as it is in (13). We do not show here this derivation as it is quite similar to developed in Ref. 28.

For completeness of the presentation we give the operators Φ_1 in details and also provide a background of BM3D filtering.

The filtering at the sensor in Step 2 is defined as $u^{t+1/2}_{s,\lambda} = \Phi_1(u^t_{s,\lambda},\, z_{s,\lambda})$, that means

$$u^{t+1/2}_{s,\lambda} = w \cdot \frac{u^t_{s,\lambda}}{|u^t_{s,\lambda}|}. \tag{17}$$

Here the ratio $\frac{u^t_{s,\lambda}}{|u^t_{s,\lambda}|}$ means that the variables $u^t_{s,\lambda}$ and $u^{t+1/2}_{s,\lambda}$ have identical phases. The amplitude w is calculated as

$$w = \frac{|u^t_{s,\lambda}| + \sqrt{|u^t_{s,\lambda}|^2 + 4z_{s,\lambda}\gamma_1(1+\gamma_1\chi)}}{2(1+\gamma_1\chi)} \tag{18}$$

Table 1. Multiwavelength APR Algorithm

	Input: $\{z_{s,\lambda}\}$, $s = 1, ..., S$, $\lambda \in \Lambda$,
	Initialization: $u^1_{o,\lambda}$, $\lambda \in \Lambda$
	Main iterations: $t = 1, 2, ..., T$
1.	**Forward propagation**:
	$u^t_{s,\lambda} = \mathcal{P}_s u^t_{o,\lambda}$, $s = 1, ..., S$, $\lambda \in \Lambda$;
2.	**Noise suppression and update of** $u^t_{s,\lambda}$:
	$u^{t+1/2}_{s,\lambda} = \Phi_1(u^t_{s,\lambda}, z_{s,\lambda})$;
3.	**Backward propagation and filtering:**
	$u^{t+1/2}_{o,\lambda} = \Phi_2(u^{t+1/2}_s)$, $u^{t+1}_{o,\lambda} = BM3D(u^{t+1/2}_{o,\lambda})$;
4.	**Absolute phase retrieval and filtering:**
	$\{\varphi^{t+1/2}_o\} = \mathcal{APR}(u^{t+1}_{o,\lambda})$,
	$\varphi^{t+1}_o = BM3D(\varphi^{t+1/2}_o)$
5.	**Object wavefront update:**
	$u^{t+1}_{o,\lambda} = \lvert u^{t+1}_{o,\lambda}\rvert \exp(j\varphi^{t+1}_o \mu_\lambda)$, $\lambda \in \Lambda$;
	Output: φ^{T+1}_o, $u^{T+1}_{o,\lambda}$.

Sparsity and BM3D filtering

The sparsity rationale assumes that there is a transform of image /signal such that it can be represented with a small number of transform coefficients or in a bit different terms with a small number of basic functions.[52] This idea is confirmed and supported by a great success of many sparsity based techniques developed for image/signal processing problems. Overall, the efficiency of the sparsity depends highly on selection of the transforms, i.e. basic functions relevant to the problem at hand. The so-called group-wise sparsity was proposed where similar patches of image are grouped and processed together (19). It is obvious that the similarity inside the groups enhances the sparsity potential.

Within the framework of nonlocal group-wise sparse image modeling, a family of the BM3D algorithms has been developed where the both ideas grouping of similar patches and the transform design are taken into consideration. This type of the algorithms proposed initially for image denoising[49] being modified for various problems demonstrate the state-of-the-art performance.[53,54]

Let us recall some basic ideas of this popular BM3D technique. At the first stage the image is partitioned into small overlapping square patches. For each patch a group of similar patches is collected which are stacked together and form a 3D array (group). This stage is called *grouping*. The entire 3D group-array is projected onto a 3D transform basis. The obtained spectral coefficients are hard-thresholded and the inverse 3D transform gives the filtered patches, which are returned to the original position of these patches in the image. This stage is called *collaborative* filtering. This process is repeated for all pixels of the entire wavefront and obtained overlapped filtered patches are aggregated in the final image estimate. This last stage is called *aggregation*. The details of BM3D as an advanced image filter can be seen in Ref. 49.

It follows from Refs. 55 and 56, that the above operations including the *grouping* define the analysis and synthesis transforms which can be combined in a single algorithm. The notation BM3D is used for this filtering algorithm.

In Step 3 of the proposed algorithm, $u^{t+1}_{o,\lambda} = BM3D(u^{t+1/2}_{o,\lambda})$, the BM3D is applied to the complex-valued variables $u^{t+1/2}_{o,\lambda}$. It is implemented in this paper as independent filtering of amplitude and wrapped phase:

$$\begin{aligned} \lvert u^{t+1}_{o,\lambda}\rvert &= BM3D_{ampl}(\lvert u^{t+1/2}_{o,\lambda}\rvert), \\ \psi^{t+1}_{o,\lambda} &= BM3D_{phase}(\psi^{t+1/2}_{o,\lambda}), \end{aligned} \tag{19}$$

here $\psi_{o,\lambda}^{t+1/2} = \text{angle}(u_{o,\lambda}^{t+1/2})$, thus the updated the complex-valued $u_{o,\lambda}^{t+1}$ is calculated as $u_{o,\lambda}^{t+1} = |u_{o,\lambda}^{t+1}| \exp(j \cdot \psi_{o,\lambda}^{t+1})$.

The novel forms of BM3D based filtering for complex-valued variables can be seen in Ref. 57.

In Step 4 of the proposed algorithm, $\varphi_o^{t+1} = BM3D(\varphi_o^{t+1/2})$, the BM3D is applied for filtering of the real-valued variable φ_o.

In our experiments the parameters of the algorithm are fixed for all tests. The parameters defining the iterations of the algorithm are as follows: $\gamma_1 = 1/\chi$, where χ is the parameter of the Poissonian distribution, $\gamma_1/\gamma_2 = 0.2$. The parameters of BM3D filters can be seen in Ref. 28.

4. NUMERICAL EXPERIMENTS

4.1 Experimental setup

In numerical experiments we model a lensless optical system (Fig. 1), where a thin transparent phase object is illuminated by monochromatic three color (RGB) coherent light beams from lasers or LEDs. The wavelengths are $\Lambda = [417,\ 532,\ 633]$ nm, with the corresponding refractive indexes [1.528, 1.519, 1.515] as taken for BK7 optical glass. The reference wavelength $\lambda' = 417$ nm then the relative frequencies take values $\mu_\lambda = [0.6425,\ 0.7705,\ 1]$. The pixel sizes of CMOS camera and SLM are 1.4 and 5.6 μm, respectively. The distance d between the object and CMOS camera is equal to 5 mm.

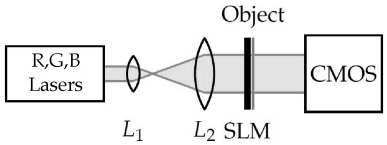

Figure 1. Optical setup. R, G, B lasers – red, green and blue light sources, L_1, L_2 – lenses, SLM – Spatial Light Modulator, CMOS – registration camera.

The free propagation of the wavefronts to the sensor is given by the Rayleigh-Sommerfeld model with the transfer function defined through the angular spectrum (AS).[58]

For the proper numerical AS propagation without aliasing effects, we introduce the zero-padding of the object obtained from the inequality:[59]

$$d \leq \frac{N \Delta x^2}{\lambda}, \tag{20}$$

which binds the propagation distance d, the number of pixels N in one dimension of the zero-padded object and the pixel size of the sensor Δx. For the distance $d = 5$ mm and the object 100×100 pixels the zero-padded object has as a support 1700×1700 pixels.

The intensities of the light beams registered on the sensor are calculated as $z_{s,\lambda} = \mathcal{G}\{|\mathcal{AS}_{\lambda,d}\{M_s \circ u_{o,\lambda}\}|^2\}$, $s = 1, ..., S$, $\lambda \subset \Lambda$.

Here $\mathcal{AS}_{\lambda,d}$ denotes the AS propagation operator and M_s are the modulation phase masks inserted before the object and pixelated as the object, $'\circ'$ stands for the pixel-wise multiplication of the object and phase masks. These phase masks enable strong diffraction of the wave-field and are introduced in order to achieve the phase diversity sufficient for reconstruction of the complex-valued object from intensity measurements. As it was described in Ref. 30 we use the Gaussian random phase masks.

Thus, in our experiments the propagation operator $\mathcal{P}_{s,\lambda,d}$ in (4) is implemented as a combination of the angular spectrum propagation $\mathcal{AS}_{\lambda,d}$ and the modulation phase mask M_s.

4.2 Reconstruction results

The illustrating reconstructions are presented for two phase objects with the invariant amplitudes equal to 1 and the phases: Gaussian distribution (100×100) and U.S. Air Force (USAF) resolution test-target (64×64). The absolute and wrapped phases of these test-objects are shown in Fig. 2. The Gaussian and USAF phases are very different, the first one has a smooth continuous shape while the second one is discontinuous binary. The both phases are taken with the high peak-value equal to 30π rad, what corresponds to about 30 reference wavelengths λ' in variations of the profile h_o.

As a result of this high peak-value of the absolute phases, the corresponding wrapped phases are very complex with fringes overlapping for the Gaussian phase and lack of height information in the USAF test-phase. Due to this complexity the unwrapping is not possible using single frequency wrapped phases only. We show that the proposed multiwavelength algorithm is quite successful and is able to reconstruct the absolute phase even from very noisy data.

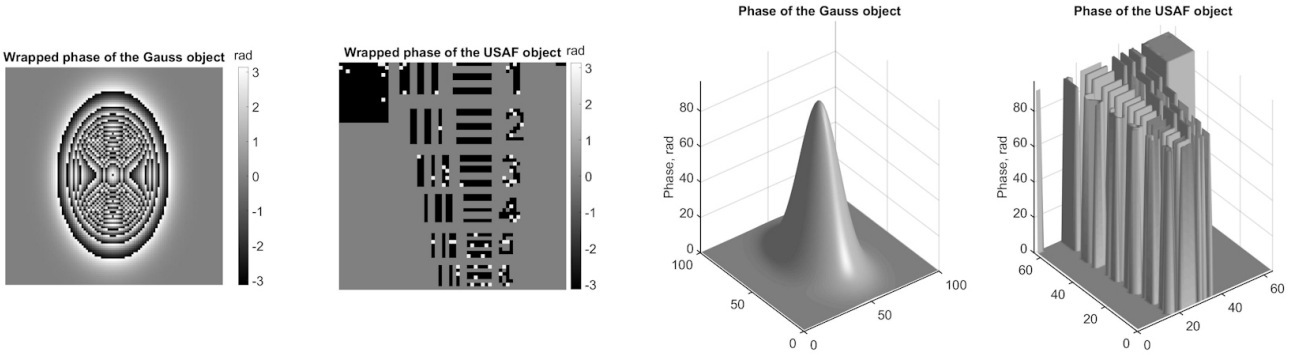

Figure 2. Wrapped and absolute phases of the investigated objects Gauss and USAF, the reference wavelength λ'=λ_1.

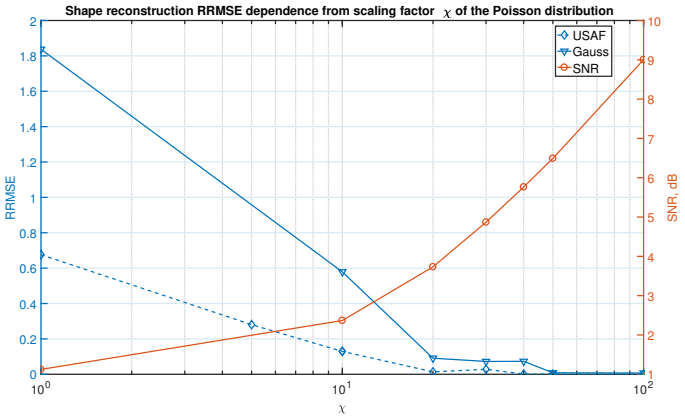

Figure 3. $RRMSE$ and SNR as function of the parameter χ of the Poissonian distribution: solid triangles and dashed diamonds curves (blue in color images) show $RRMSE$ for the Gaussian and USAF objects, respectively (left y-axis); solid circle curve (orange) shows SNR of the observations (right y-axis).

We demonstrate the performance of the multiwavelength APR algorithm for the very difficult scenarios with very noisy Poissonian observations. The noisiness of observations is characterized by SNR (10) and by the mean number of photons per sensor pixel, N_{photon} (11).

The accuracy of the object reconstruction is characterized by the Relative Root-Mean-Square Error ($RRMSE$) criteria calculated as $RMSE$ divided by the root of the mean square power of the signal:

$$RRMSE_{\varphi} = \frac{\sqrt{||\hat{\varphi}_{est} - \varphi_{true}||_2^2}}{\sqrt{||\varphi_{true}||_2^2}}, \tag{21}$$

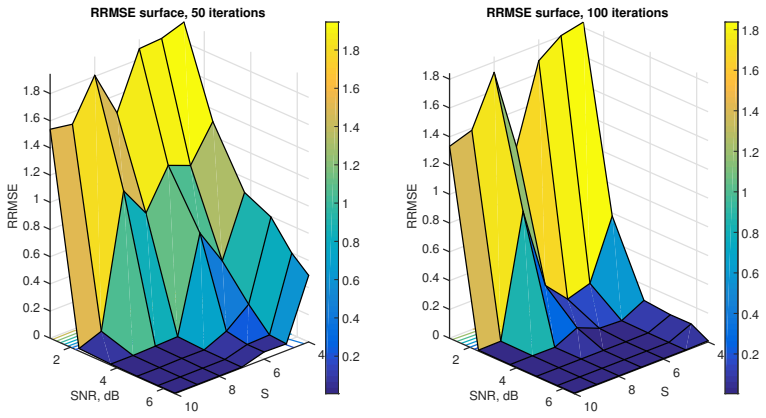

Figure 4. Gaussian object, $RRMSE$ as function of SNR and the experiment number S: after 50 and 100 iterations, left and right 3D plots, respectively.

In this criteria the phase estimate is corrected by the mean value of the error between the estimate and the true absolute phase value. It is the standard approach in evaluation of the accuracy for the phase retrieval where the phase is estimated within an invariant summand.

It is important to note that the values of RRMSE are identical for the estimation accuracy of the phase and the profile h_o. It happens because these estimates are different only by the invariant factors which are the same in the nominator and denominator of $RRMSE$.

Figure 3 shows the performance of the APR algorithm with respect to different noise levels characterized by the parameter χ. The $RRMSE$ curves for Gaussian and USAF phases demonstrate a similar behavior and go down for growing χ numbers, but $RRMSE$ curve for the USAF object goes down more sharply and takes values smaller than 0.1 at $\chi = 20$, while $RRMSE$ curve for Gaussian phase takes a close value only at $\chi = 50$. Nevertheless, in the both cases, the reconstructions are nearly perfect even for very noisy observed data with SNR values as low as 3.8 and 6.5 dB and very small photon numbers $N_{photon} = 0.75$ and 1.87, respectively.

$RRMSEs$ for the Gaussian phase are shown in Fig. 4 as functions of the experiments number S and SNR. Nearly horizontal areas (dark blue) areas correspond to high-accuracy reconstructions with small values of $RRMSE$, for other areas $RRMSE$ values are much higher and the accuracy is not so good. For 50 iterations (left image) the high accuracy can be achieved starting from $S = 8$ even for very noisy data with $SNR = 4$. For $S = 4$ good results can be obtained only after 100 iterations (right image). It follows from Fig. 4 that some improvement in the accuracy can be achieved at the price on the larger number of experiments S and the larger number of iterations. In what follows, we provide the images of the reconstructed absolute phase obtained for $S = 4$ and the iteration number $T = 100$.

Figures 5 and 6 illustrate absolute phase reconstructions (3D/2D images) obtained by the multiwavelength APR algorithm and by the SPAR algorithm reconstructing the wrapped phases for the separate wavelengths following by the phase unwrapping by the PUMA phase unwrapping algorithm.[38] The conditions of the experiments are: $SNR = 6.5$ dB, $N_{photon} = 1.87$ for Gaussian object and $SNR = 3.8$ dB, $N_{photon} = 0.75$ for the USAF object. The multiwavelength APR algorithm demonstrates a strong ability to reconstruct the absolute phases while the single wavelength based approach completely failed. The accuracy of the APR reconstruction is very high despite of a high level of the noise.

The wrapped phase pattern for such high peak-value of the object phases is very complex and irregular (see Fig.2) that it is not possible to unwrap it by modern 2D unwrapping algorithms, but proposed algorithm is able to resolve the problem even for such complex case. Especially it is challenging task to reconstruct objects like USAF with big differences between adjacent pixels exceeding 2π, but the APR algorithm successfully reconstruct both objects with high reconstruction quality.

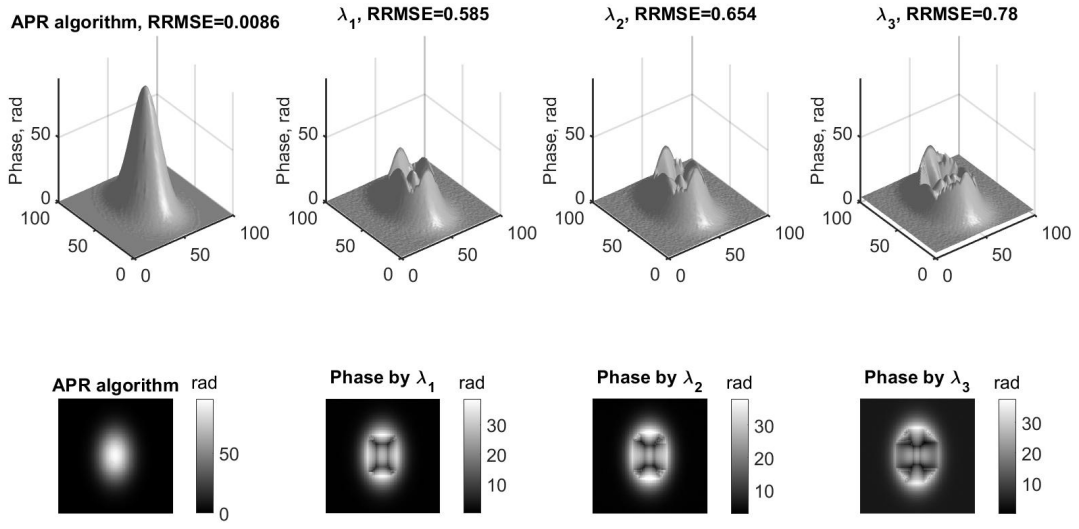

Figure 5. Gaussian phase reconstructions $RRMSE = 0.0086$ for $SNR = 6.5$ dB ($N_{photon} = 1.87$), top row - 3D surfaces, bottom row - 2D absolute phases. From left to right: algorithm APR, and λ_1, λ_2, λ_3 wavelengths, respectively.

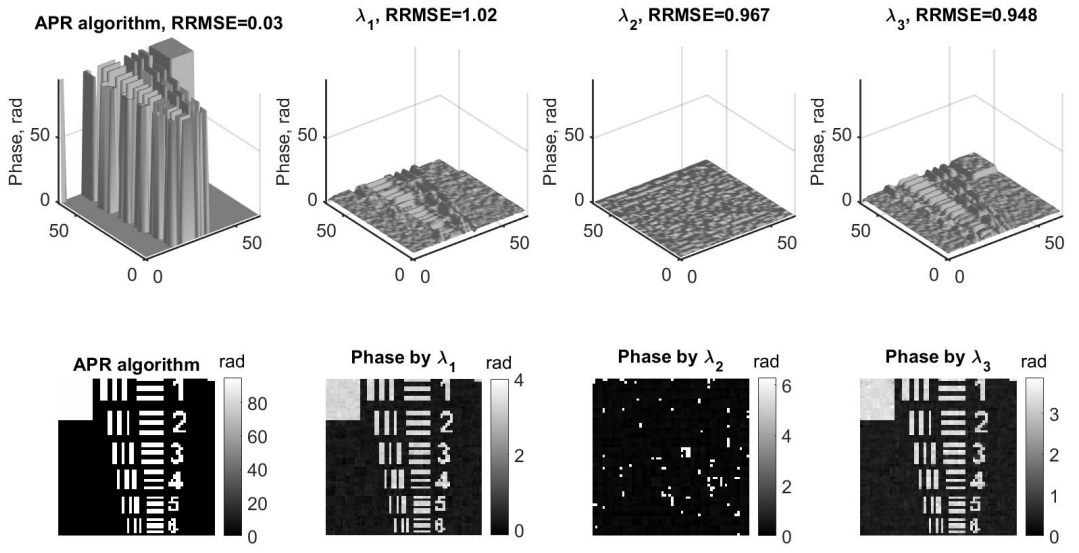

Figure 6. USAF phase reconstructions $RRMSE = 0.030$ for $SNR = 3.8$ dB ($N_{photon} = 0.75$), top row - 3D surfaces, bottom row - 2D absolute phases. From left to right: algorithm APR, and λ_1, λ_2, λ_3 wavelengths, respectively.

For simulations we use MATLAB R2016b on a computer with 32 GB of RAM and CPU with a 3.40 GHz Intel® Core™ i7-3770 processor. The computation complexity of the algorithm is characterized by the time required for processing. For 1 iteration, $S = 4$, and 100×100 pixels images, zero-padded to 1700×1700, this time equals to 12 s.

5. CONCLUSION

The multiwavelength absolute phase retrieval from noisy intensity observations is considered. The maximum likelihood criterion used in the developed multi-objective optimization (Nash equilibrium technique) defines the intention to reach statistically optimal estimates. The phase retrieval is an ill-posed inverse problem where the observation noise is amplified and transferred to phase and amplitude as variables of optimization. The sparse modeling enables a regularization of this inverse problem and efficient suppression of these random errors by BM3D filtering of phase and amplitude. The efficiency of the developed APR algorithm is demonstrated by simulation experiments for the coded diffraction pattern scenario.

Acknowledgments

This work is supported by Academy of Finland, project no. 287150, 2015-2019, Russian Ministry of Education and Science (project within the state mission for institutions of higher education, agreement 3.1893.2017/4.6) and Horizon 2020 TWINN-2015, grant 687328 - HOLO.

Appendix

Absolute phase reconstruction (APR) algorithm.

The minimization of $\mathcal{L}_1$ (16) on φ_o and δ_λ is an absolute phase estimation (unwrapping) problem where the joint use of the λ-channels is required.

The algorithm is composed from three successive stages A, B, C. We name this algorithm *Absolute phase reconstruction (APR) algorithm.*

(A) *Phase synchronization.* Let $\lambda' \in \Lambda$ be a reference channel. Define δ_λ for (16) in the following way

$$\hat{\delta}_\lambda = \mathcal{W}(\hat{\delta}_{\lambda'} \cdot \mu_\lambda/\mu_{\lambda'} + \delta_{\lambda,\lambda'}\mu_\lambda), \tag{22}$$

where $\delta_{\lambda,\lambda'}$ define the shifts between the phases of the reference and other channels:

$$\delta_{\lambda,\lambda'} = median_x(\mathcal{W}(\psi_{o,\lambda}(x)/\mu_\lambda - \psi_{o,\lambda'}(x)/\mu_{\lambda'})) \tag{23}$$

and $\hat{\delta}_{\lambda'}$ is a hypothetical valued of unknown $\delta_{\lambda'}$. One of the goals of this calculations is to reduce a number of unknown phase shifts δ_λ to a single parameter $\delta_{\lambda'}$, i.e. the phase-shift in the reference channel. Note that in the above formulas $\psi_{o,\lambda}(x)$ are known (measured) in the algorithm iterations. Thus, indeed, all δ_λ are expressed through $\hat{\delta}_{\lambda'}$. The wrapping operator $\mathcal{W}$ in (22)-(23) is used for proper calculation of the wrapped phase and the median averaging in order to get the robust estimate of the invariant $\delta_{\lambda,\lambda'}$.

Inserting $\hat{\delta}_\lambda$ in (16) we obtain this criterion in the form

$$\mathcal{L}_1(\varphi\,,\ \delta_\lambda) = \sum_\lambda |||u_{o,\lambda}|[\exp(j(\mu_\lambda \cdot \varphi_o)) - \exp(j(\psi_{o,\lambda} - \hat{\delta}_{\lambda'} \cdot \mu_\lambda/\mu_{\lambda'} - \delta_{\lambda,\lambda'}\mu_\lambda))]||_2^2, \tag{24}$$

where $\delta_{\lambda,\lambda'}$ is given.

The meaning of $\mathcal{L}_1(b_{o,\lambda},\ \varphi\,,\ \delta_\lambda)$ can be revealed if we drop all these operations and assume that all phase manipulations are accurate than we can see that

$$\psi_{o,\lambda} - \hat{\delta}_\lambda = \mu_\lambda \cdot \varphi_o + \delta_\lambda - \hat{\delta}_\lambda,$$
$$\hat{\delta}_\lambda = \delta_\lambda + \mu_\lambda/\mu_{\lambda'}(\hat{\delta}_{\lambda'} - \delta_\lambda).$$

It follows

$$\psi_{o,\lambda} - \hat{\delta}_\lambda = \mu_\lambda \cdot \varphi_o + \mu_\lambda/\mu_{\lambda'}(\hat{\delta}_{\lambda'} - \delta_{\lambda'}). \tag{25}$$

If we know that $\delta_{\lambda'} = \hat{\delta}_{\lambda'}$ than the perfect phase equalization is produced and $\psi_{o,\lambda} - \hat{\delta}_\lambda = \mu_\lambda \cdot \varphi_o$. In general case when $\delta_{\lambda'} \neq \hat{\delta}_{\lambda'}$, the in-phase situation is not achieved.

Going back to the criterion (24) we note that with this compensation it takes the form

$$\mathcal{L}_1(\varphi_o\,,\ \delta_\lambda) = \sum_\lambda |||u_{o,\lambda}|[\exp(j(\mu_\lambda \cdot \varphi_o)) - \exp(j(\psi_{o,\lambda} - \hat{\delta}_\lambda))]||_2^2. \tag{26}$$

and using (25) it can be rewritten as

$$\mathcal{L}_1(\varphi_o\,,\ \delta_\lambda) = \sum_\lambda |||u_{o,\lambda}|[\exp(j(\mu_\lambda(\varphi_o + \Delta\varphi_o)) - \exp(j(\psi_{o,\lambda} - \delta_\lambda))]||_2^2,\ \Delta\varphi_o = (\hat{\delta}_{\lambda'} - \delta_{\lambda'})/\mu_{\lambda'}.$$

Thus, the accurate compensation of the phase shifts δ_λ in the wrapped phases $\psi_{o,\lambda}$ is achieved while the absolute phase φ_o can be estimated within an unknown but invariant phase shift $\Delta\varphi_o$. In principle, this is not essential summand as in any case by default the phase retrieval setup φ_o can be estimated only within an invariant shift. However, it is noticed that minimization on $\delta_{\lambda'}$ allows to improve essentially the accuracy of the absolute phase reconstruction.

The equivalence of the calculations (22)-(23) to the phase manipulations shown in (25) cannot be proved analytically but careful numerical experiments confirm that they are quite precise even for noisy data.

(B) *Minimization of* (26) *on* φ_o is a solution of the problem

$$\hat{\varphi}_o(x,\ \delta_{\lambda'}) = \arg\min_{\varphi_o(x)} \mathcal{L}_1(\varphi_o\,,\ \hat{\delta}_\lambda), \tag{27}$$

$$\hat{\delta}_\lambda = \hat{\delta}_{\lambda'} \cdot \mu_\lambda/\mu_{\lambda'} + \delta_{\lambda,\lambda'}\mu_\lambda, \tag{28}$$

where

$$\mathcal{L}_1(\varphi_o,\ \hat{\delta}_\lambda) = 2\sum_\lambda \sum_x |u_{o,\lambda}(x)|^2[1 - \cos(\mu_\lambda \cdot \varphi_o(x) - (\psi_{o,\lambda}(x) - \hat{\delta}_\lambda))]. \tag{29}$$

Minimization of (29) *on* φ_o gives the estimate of the absolute phase provided give $\hat{\delta}_\lambda$. It has no an analytical solution and is obtained by numerical calculations.

The calculations in (29) are produced pixel-wise for each pixel x independently. Note that $\hat{\delta}_\lambda$ as well as the solution $\hat{\varphi}_o$ both depend on the unknown invariant $\hat{\delta}_{\lambda'}$.

(C) *Minimization of* (29) on $\delta_{\lambda'}$ leads to the following scalar numerical optimization:

$$\hat{\delta}_{\lambda'} = \min_{\delta_{\lambda'}} \sum_\lambda \sum_x |u_{o,\lambda}|^2[1 - \cos(\mu_\lambda \cdot \hat{\varphi}_o(x, \delta_{\lambda'}) - (\psi_{o,\lambda}(x) - (\delta_{\lambda'} \cdot \mu_\lambda/\mu_{\lambda'} + \delta_{\lambda,\lambda'}\mu_\lambda))]. \tag{30}$$

Finalization of estimation. When $\hat{\delta}_{\lambda'}$ is found the optimal values for $\hat{\varphi}_o$ are calculated as

$$\hat{\varphi}_o(x) = \hat{\varphi}_o(x, \hat{\delta}_{\lambda'}). \tag{31}$$

In our algorithm implementation the solutions for (27) and (30) are obtained by the grid optimization.

REFERENCES

[1] Picart, P. and Li, J., [*Digital holography*], John Wiley & Sons (2013).

[2] Schnars, U., Falldorf, C., Watson, J., and Jüptner, W., [*Digital Holography and Wavefront Sensing*] (2015).

[3] Belashov, A. V., Beltyukova, D. M., Vasyutinskii, O. S., Petrov, N. V., Semenova, I. V., and Chupov, A. S., "Holographic monitoring of spatial distributions of singlet oxygen in water," *Technical Physics Letters* **40**(12), 1134–1135 (2014).

[4] Almoro, P. F., Pedrini, G., Gundu, P. N., Osten, W., and Hanson, S. G., "Enhanced wavefront reconstruction by random phase modulation with a phase diffuser," *Optics and Lasers in Engineering* **49**(2), 252–257 (2011).

[5] Candès, E. J., Li, X., and Soltanollotabi, M., "Phase Retrieval from Coded Difraction Patterns," *Arxiv* **2013**, 1–24 (2013).

[6] Almoro, P. F., Pham, Q. D., Serrano-Garcia, D. I., Hasegawa, S., Hayasaki, Y., Takeda, M., and Yatagai, T., "Enhanced intensity variation for multiple-plane phase retrieval using a spatial light modulator as a convenient tunable diffuser," *Optics Letters* **41**(10), 2161 (2016).

[7] Camacho, L., Micó, V., Zalevsky, Z., and García, J., "Quantitative phase microscopy using defocusing by means of a spatial light modulator.," *Optics express* **18**(7), 6755–6766 (2010).

[8] Kress, Bernard C., M. P., [*Applied Digital Optics - From Micro optics to Nanophotonics*], John Wiley & Sons (2009).

[9] Gerchberg, R. W. and Saxton, W. O., "A Practical Algorithm for the Determination of Phase from Image and Diffraction Plane Pictures," *Phys. E. ppl. Opt. OPTIK* **2**(352), 237–246 (1969).

[10] Fienup, J. R., "Phase retrieval algorithms: a comparison," *Applied Optics* **21**, 2758 (8 1982).

[11] Shevkunov, I. A., Balbekin, N. S., and Petrov, N. V., "Comparison of digital holography and iterative phase retrieval methods for wavefront reconstruction," in [*SPIE/COS Photonics Asia, Holography, Diffractive Optics, and Applications VI*], Sheng, Y., Yu, C., and Zhou, C., eds., **9271**, 927128 (11 2014).

[12] Gaur, C., Mohan, B., and Khare, K., "Sparsity-assisted solution to the twin image problem in phase retrieval," *Journal of the Optical Society of America A* **32**, 1922 (11 2015).

[13] Guo, C., Liu, S., and Sheridan, J. T., "Iterative phase retrieval algorithms I: optimization," *Applied Optics* **54**(15), 4698 (2015).

[14] Fienup, J. R., "Phase-retrieval algorithms for a complicated optical system," *Applied Optics* **32**(10), 1737 (1993).

[15] Bauschke, H. H., Combettes, P. L., and Luke, D. R., "Phase retrieval, error reduction algorithm, and Fienup variants: a view from convex optimization," *Journal of the Optical Society of America A* **19**(7), 1334 (2002).

[16] Pauwels, E. J. R., Beck, A., Eldar, Y. C., and Sabach, S., "On Fienup Methods for Sparse Phase Retrieval," *IEEE Transactions on Signal Processing* **66**, 982–991 (2 2018).

[17] Shechtman, Y., Eldar, Y. C., Cohen, O., Chapman, H. N., Miao, J., and Segev, M., "Phase Retrieval with Application to Optical Imaging: A contemporary overview," *IEEE Signal Processing Magazine* **32**, 87–109 (5 2015).

[18] Candès, E. J., Eldar, Y. C., Strohmer, T., and Voroninski, V., "Phase Retrieval via Matrix Completion," *SIAM Review* **57**, 225–251 (1 2015).

[19] Shechtman, Y., Beck, A., and Eldar, Y. C., "GESPAR: Efficient phase retrieval of sparse signals," *IEEE Transactions on Signal Processing* **62**(4), 928–938 (2014).

[20] Yurtsever, A., Udell, M., Tropp, J. A., and Cevher, V., "Sketchy Decisions: Convex Low-Rank Matrix Optimization with Optimal Storage," *arxiv.org* (2 2017).

[21] Candès, E. J., Li, X., and Soltanolkotabi, M., "Phase Retrieval via Wirtinger Flow: Theory and Algorithms," *Information Theory, IEEE Transactions on* **61**(4), 1985–2007 (2015).

[22] Chen, Y. and Candès, E. J., "Solving Random Quadratic Systems of Equations Is Nearly as Easy as Solving Linear Systems," *Communications on Pure and Applied Mathematics* **70**(5), 822–883 (2017).

[23] Weller, D. S., Pnueli, A., Divon, G., Radzyner, O., Eldar, Y. C., and Fessler, J. A., "Undersampled Phase Retrieval With Outliers," *IEEE Transactions on Computational Imaging* **1**, 247–258 (12 2015).

[24] Soulez, F., Thiébaut, ., Schutz, A., Ferrari, A., Courbin, F., and Unser, M., "Proximity operators for phase retrieval," *Applied Optics* **55**(26), 7412 (2016).

[25] Katkovnik, V. and Astola, J., "High-accuracy wave field reconstruction: decoupled inverse imaging with sparse modeling of phase and amplitude," *Journal of the Optical Society of America A* **29**(1), 44–54 (2012).

[26] Katkovnik, V. and Astola, J., "Compressive sensing computational ghost imaging," *Journal of the Optical Society of America A* **29**(8), 1556 (2012).

[27] Katkovnik, V. and Astola, J., "Sparse ptychographical coherent diffractive imaging from noisy measurements.," *Journal of the Optical Society of America. A, Optics, image science, and vision* **30**(3), 367–79 (2013).

[28] Katkovnik, V., "Phase retrieval from noisy data based on sparse approximation of object phase and amplitude," *arxiv* , 1–16 (9 2017).

[29] Katkovnik, V. and Egiazarian, K., "Sparse superresolution phase retrieval from phase-coded noisy intensity patterns," *Optical Engineering* **56**, 1 (9 2017).

[30] Katkovnik, V., Shevkunov, I., Petrov, N. V., and Egiazarian, K., "Computational super-resolution phase retrieval from multiple phase-coded diffraction patterns: simulation study and experiments," *Optica* **4**, 786 (7 2017).

[31] Tillmann, A. M., Eldar, Y. C., and Mairal, J., "DOLPHIn - Dictionary Learning for Phase Retrieval," *IEEE Transactions on Signal Processing* **64**(24), 6485–6500 (2016).

[32] Pedrini, G., Osten, W., and Zhang, Y., "Wave-front reconstruction from a sequence of interferograms recorded at different planes.," *Optics letters* **30**(8), 833–835 (2005).

[33] Falldorf, C., Huferath-von Luepke, S., von Kopylow, C., and Bergmann, R. B., "Reduction of speckle noise in multiwavelength contouring," *Applied Optics* **51**(34), 8211 (2012).

[34] Towers, C. E., Towers, D. P., and Jones, J. D. C., "Absolute fringe order calculation using optimised multi-frequency selection in full-field profilometry," *Optics and Lasers in Engineering* **43**(7), 52–64 (2005).

[35] Tahara, T., Otani, R., Arai, Y., and Takaki, Y., "Multiwavelength Digital Holography and Phase-Shifting Interferometry Selectively Extracting Wavelength Information: Phase-Division Multiplexing (PDM) of Wavelengths," in [*Holographic Materials and Optical Systems*], Ch. 09, InTech (3 2017).

[36] Claus, D., Pedrini, G., and Osten, W., "Iterative phase retrieval based on variable wavefront curvature," *Applied Optics* **56**, F134 (5 2017).

[37] Bioucas-Dias, J., Katkovnik, V., Astola, J., and Egiazarian, K., "Multi-frequency Phase Unwrapping from Noisy Data: Adaptive Local Maximum Likelihood Approach RID C-5479-2009," *Image Analysis, Proceedings* **5575**, 310–320 (2009).

[38] Bioucas-Dias, J. and Valadão, G., "Multifrequency absolute phase estimation via graph cuts," in [*European Signal Processing Conference*], 1389–1393 (2009).

[39] Bao, P., Zhang, F., Pedrini, G., and Osten, W., "Phase retrieval using multiple illumination wavelengths," *Opt. Lett.* **33**(4), 309–311 (2008).

[40] Petrov, N. V., Bespalov, V. G., and Gorodetsky, A. a., "Phase retrieval method for multiple wavelength speckle patterns," *Proc. of SPIE* **7387**, 73871T–73871T–7 (2010).

[41] Petrov, N. V., Volkov, M. V., Gorodetsky, A. a., and Bespalov, V. G., "Image reconstruction using measurements in volume speckle fields formed by different wavelengths," *Proc. SPIE* **7907**, 790718–790718 (2011).

[42] Bao, P., Situ, G., Pedrini, G., and Osten, W., "Lensless phase microscopy using phase retrieval with multiple illumination wavelengths.," *Applied optics* **51**(22), 5486–94 (2012).

[43] Phillips, Z. F., Chen, M., and Waller, L., "Single-shot quantitative phase microscopy with color-multiplexed differential phase contrast (cDPC)," *PLOS ONE* **12**, e0171228 (2 2017).

[44] Sanz, M., Picazo-Bueno, J. A., García, J., and Micó, V., "Improved quantitative phase imaging in lensless microscopy by single-shot multi-wavelength illumination using a fast convergence algorithm," *Optics Express* **23**(16), 21352–21365 (2015).

[45] Falaggis, K., Towers, D. P., and Towers, C. E., "Algebraic solution for phase unwrapping problems in multiwavelength interferometry," *Applied optics* **53**(17), 3737 (2014).

[46] Wang, W., Li, X., Wang, W., and Xia, X. G., "Maximum likelihood estimation based Robust Chinese remainder theorem for real numbers and its fast algorithm," *IEEE Transactions on Signal Processing* **63**(13), 3317–3331 (2015).

[47] Xiao, L., Xia, X.-G., and Huo, H., "Towards Robustness in Residue Number Systems," *IEEE Transactions on Signal Processing* **65**, 1–32 (3 2016).

[48] Kulya, M. S., Balbekin, N. S., Gredyuhina, I. V., Uspenskaya, M. V., Nechiporenko, A. P., and Petrov, N. V., "Computational terahertz imaging with dispersive objects," *Journal of Modern Optics* **64**, 1283–1288 (7 2017).

[49] Dabov, K., Foi, A., and Katkovnik, V., "Image denoising by sparse 3D transformation-domain collaborative filtering," *IEEE Transactions on Image Processing* **16**(8), 1–16 (2007).

[50] Raginsky, M., Willett, R., Harmany, Z., and Marcia, R., "Compressed sensing performance bounds under Poisson noise," *Signal Processing, IEEE Transactions on* **58**(8), 39904002 (2010).

[51] Harmany, Z. T., Marcia, R. F., and Willett, R. M., "Sparsity-regularized photon-limited imaging," in [*2010 IEEE International Symposium on Biomedical Imaging: From Nano to Macro*], 772–775, IEEE (2010).

[52] Mallat, S. G., "A Theory for Multiresolution Signal Decomposition: The Wavelet Representation," *IEEE Transactions on Pattern Analysis and Machine Intelligence* **11**(7), 674–693 (1989).

[53] Rajwade, A., Rangarajan, A., and Banerjee, A., "Image Denoising Using the Higher Order Singular Value Decomposition," *IEEE Transactions on Pattern Analysis and Machine Intelligence* **35**, 849–862 (4 2013).

[54] Metzler, C. A., Maleki, A., and Baraniuk, R. G., "BM3D-PRGAMP: Compressive phase retrieval based on BM3D denoising," in [*2016 IEEE International Conference on Image Processing (ICIP)*], 2504–2508, IEEE (9 2016).

[55] Danielyan, A., Katkovnik, V., and Egiazarian, K., "BM3D Frames and Variational Image Deblurring," *IEEE Transactions on Image Processing* **21**, 1715–1728 (4 2012).

[56] Katkovnik, V., Shevkunov, I. A., Petrov, N. V., and Egiazarian, K., "Wavefront reconstruction in digital off-axis holography via sparse coding of amplitude and absolute phase," *Optics Letters* **40**(10), 2417 (2015).

[57] Katkovnik, V., Ponomarenko, M., and Egiazarian, K., "Sparse approximations in complex domain based on BM3D modeling," *Signal Processing* **141**, 96–108 (2017).

[58] Goodman, J. W., [*Introduction to Fourier optics*], Roberts & Co (2005).

[59] Petrov, N. V., Bespalov, V. G., and Volkov, M. V., "Phase retrieval of THz radiation using set of 2D spatial intensity measurements with different wavelengths," *Proc. of SPIE* **8281**(February), 82810J–82810J–7 (2012).